Duplex steel welding in artic conditions – Correlation of welding parameters in relation to HISC

To cite this article: Z Czarnacki and Y Xing 2021 *IOP Conf. Ser.: Mater. Sci. Eng.* **1201** 012016

Duplex steel welding in artic conditions – Correlation of welding parameters in relation to HISC

Z Czarnacki[1, 2] and Y Xing[1,*]

[1] University of Stavanger, Norway
[2] MEWO Subsea Solutions, Poland

[*] Contact author: yihan.xing@uis.no

Abstract. Duplex steel is an austenitic-ferritic steel alloy commonly used in the offshore and subsea oil and gas industry. Duplex steel provides a unique combination of good mechanical properties and corrosion resistance in sweet and sour hydrocarbon environment, as well as in seawater. However, the combination of tensile loading, post-weld residual stresses, cathodic protection and other factors related to subsea implementation significantly increase the probability of hydrogen induced stress cracking (HISC). This paper aims to find a relationship between the formation of residual stresses and the imperfection of the welding process carried out on Duplex steel in extremely cold conditions. Based on a finite element (FE) welding transient simulation from a thermal perspective, the correlation between the welding parameters and heat distribution is established and analysed when the welding takes place in the cold arctic conditions. Pearson parameter correlation analysis method will be used to investigate the impact of extreme ambient temperatures on the welding process. The results and conclusions provide a solid foundation for welding process optimization in connection with HISC.

1. Introduction

One of the most used materials in the offshore and subsea industry is the austenitic-ferritic alloy, Duplex steel. The extreme environmental conditions found at the bottom of the seas and oceans require the use of material resistant to corrosion, as well as aggressive chemicals found in hydrocarbons that are transported and processed at the seabed. All these requirements must be met while maintaining superb mechanical strength. The subsea installations are subjected to high pressure and temperature gradients, vibrations, and accidental loads. Although the cost of Duplex steel is very high, its specific properties in providing good mechanical properties in combination with good corrosion resistance make its use substantiated. Using Duplex steel can reduce structural weight, maintenance costs and increase the system lifetime, resulting in a long-term cost reduction. Fulfilling all the previously mentioned requirements made the Duplex steel a very popular material for subsea equipment production [1].

Cathodic protection (CP) is normally applied as one of the main corrosion inhibition measures in subsea equipment. It is an effective corrosion inhibition method; however, CP also makes Duplex steel materials susceptible to HISC. HISC typically occurs at the heat affected zones (HAZs) of welded joints. Welding is a standard method used to join various steel sub-components to manufacture the final structure. During the welding process, large amounts of heat dissipate with high gradients around the joined seam. After cooldown, residual stresses form in the HAZ area surrounding the weld. The susceptibility to HISC is significantly influenced by the post welding residual stresses, which formation

is highly dependent to ambient temperature. Recent tendency to develop far north arctic areas such as Goliath (2017) and Johan Castberg (2022) raises the need to also focus on the influence of arctic conditions on the welding process. The scope of this paper is to investigate this phenomenon. The heat flux caused by welding will be modeled and simulated. FE simulations will be carried out both for moderate climate and extreme arctic conditions. The correlation of welding parameters will be analyzed to find the area on which the focus should be laid on. The heat distribution will be analyzed to predict formation of stresses, strains, and microstructure changes; these being key to the proper understanding and future prevention of HISC propagation in welded seams.

2. Duplex stainless steel and HISC

2.1. Background on Duplex steel

Duplex steel is made up of mainly austenite and ferrite steel in combination with a few other alloying elements such as nickel, chromium, and molybdenum. It was first developed in the 1920s in Sweden and has the following advantageous mechanical properties [2]:

- Very high yield strength (up to 550Mpa)
- High toughness in a wide range of temperatures (low and moderate)
- Good weldability
- Resistance to aggressive chemicals
- Limited susceptibility to stress corrosion cracking

These advantageous properties come with the drawbacks of high production cost and poor machinability. Furthermore, the previously mentioned superior mechanical properties are only maintained in temperatures below 300 ℃. Duplex steel is a popular material choice in offshore and subsea industry where the Duplex (S31803) and Super Duplex (S32750) grades are commonly employed. The characteristics of these metals [3] are presented in Table 1.

Table 1. Characteristics overview – Duplex and Super Duplex

Parameter	Duplex	Super Duplex
Chemical composition	22Cr-5Ni-3Mo	25Cr-7Ni-4Mo
Price	4-5 USD/kg	7-11 USD/kg
Melting point	1420-1465 ℃	1350 ℃
Mechanical strength	YS = 450 MPa US = 620 MPa	YS = 550 MPa US = 795 MPa
Resistance to stress corrosion cracking	High	Excellent
Resistance to pitting and crevice corrosion	High	Excellcent
Resistnace to general corrosion	High	High
Resistance to erosion, corrosion and corrosion fatigue	High	High
Weldability	Good	Good

When compared to a typical construction steels used in civil engineering, both Duplex and Super Duplex have a significantly higher content of alloying elements. Although, such composition provides a superb resistance to chemicals and corrosion, it limits its use in terms of temperature range. Duplex steel is mostly associated with subsea engineering, where cooling is rarely a problem. Being substantially less expensive than Super Duplex, the S31803 is usually a material of choice in deep-sea offshore projects. Super Duplex steel which has a slightly higher content of chromium (+3%),

molybdenum (+1%) and nickel (+1%) provides not only higher resistance to corrosion cracking and pitting, but also mechanical strength, when compared to the regular Duplex. It is however much more expensive. It is typically used in equipment exposed to very high pressure and temperature gradients, as well as chemicals (pressure vessels, boilers, heat exchangers, chemical processing, pressure vessels). An example of an incline valve manufactured from Super Duplex steel is presented in Figure 1.

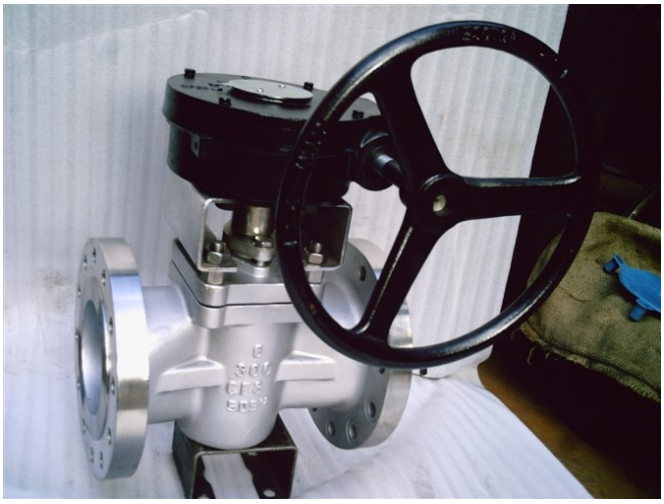

Figure 1. Plug Valve made from Super Duplex Steel (Heather Smith, 2009, Creative Commons)

2.2. Residual stresses after welding

During welding, a powerful heat flux is introduced to locally melt the material and after cool down, form a homogenous, continuous bond. Consequently, the welding process causes a rapid rise of temperature at a limited area. Depending on the physical material properties of connected components, it results in a large temperature gradient in the material section, which after rapid cooldown might cause formation of residual stresses in the area surrounding the seam (HAZ). Allotropic layers in a HAZ around a single U-type weld joint is illustrated in Figure 2. Depending on the welding method, the heat source concentration varies, and the phenomenon can have different degrees of severity [4].

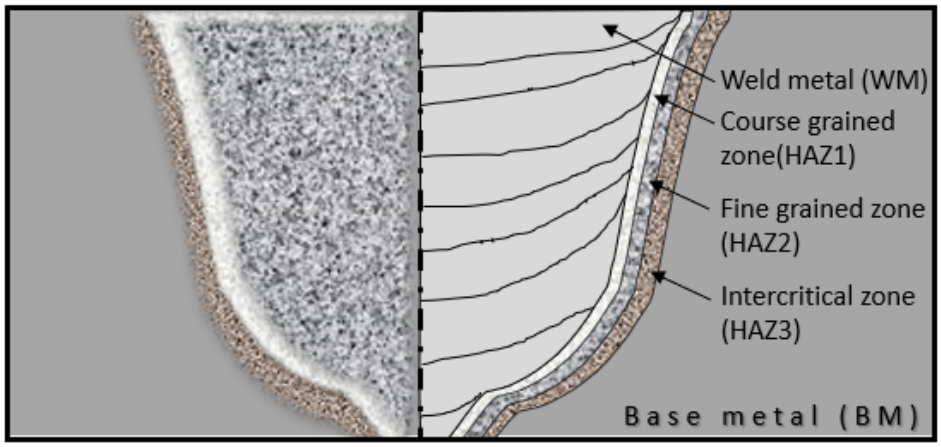

Figure 2. Allotropic layers in a HAZ around a single U-type weld joint

Large magnitudes of temperature gradients are the main cause of residual stress appearance after welding. When subjected to a powerful heat flux, the metal rapidly expands, which results in compression of further layers. Some areas remain in a solid state, the ones closer to the welding path

reach the liquid state. When melted, the metal is instantaneously relieved thanks to grain recrystallization [5]. Over the time of the weld seam cool down the microstructure of the material changes again. The relieved object in a solid state, starts to rapidly reduce its volume, which causes internal tension. The magnitude of these stresses is mostly dependent on cooldown rate. That is why the welds are typically relieved with tempering. The phenomenon is even more severe when the welded components are already fixed in place with limited degrees of freedom. Another important factor is the ambient temperature. Low ambient temperature will inflict faster cooldown, causing steeper temperature gradients in the metal section [6].

Heat treatment is a standard method to remove/reduce residual stresses caused by welding or other manufacturing processes. The main goal is to remove internal stresses and structurally homogenize the large area around the weld seam (because of recrystallisation). Such effect is achieved by an increase of temperature to a certain threshold. Once properly heated, the object must be carefully cooled down, so that the excess heat will have time to escape and not cause internal tension once again [7].

There are tools on the market that allow for precise and efficient heat treatment of weld seams. An example of such equipment is presented above. The construction of such device is rather simple. The belt is a combination of electric heaters with temperature sensors as illustrated in Figure 3. Depending on the weld type, alloy and geometry of an object a time dependent temperature profile is uploaded to the controller. That way, the temperature can be precisely adjusted for every timestep giving best results [8].

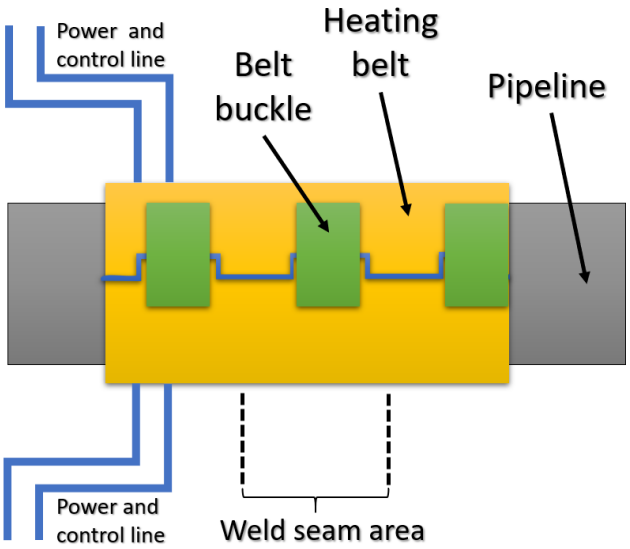

Figure 3. Annealing belt used for Post Weld Heat Treatment (PWHT) of pipe joints

Unfortunately, especially in subsea processing installations, the geometry scale and complexity of certain components limits the implementation of simple methods like the one presented in Figure 3. In these cases, the heat treatment is either limited or not possible, that's especially the case in tight closed spaces. PWHT is also a process requiring an in depth understating of metallurgy, experience, and precision. Performed incorrectly, it might give poor results, or even weaken the component, which might lead to critical failure [9].

2.3. Hydrogen induced stress cracking

For HISC phenomenon to occur, all three certain requirements must be met as illustrated in Figure 4.

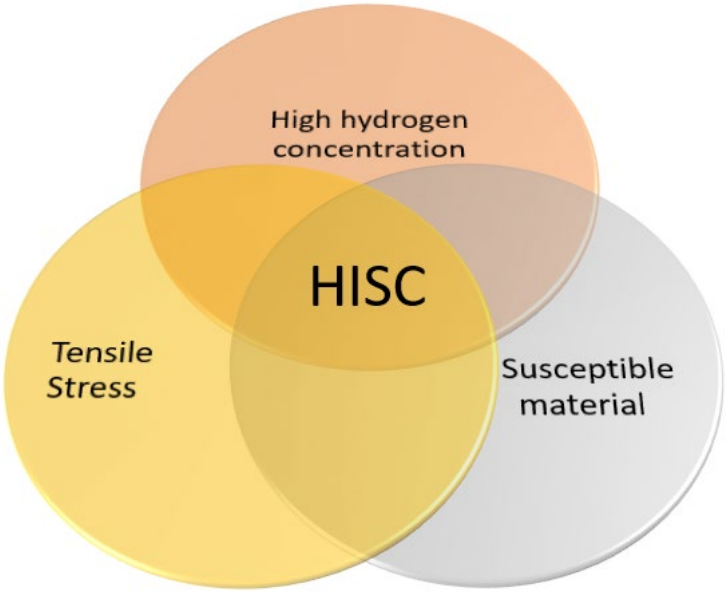

Figure 4. HISC phenomenon – necessary factors for its occurrence (Ref. DNV-RP-F101[10])

Tensile Stress: This can be caused by either mechanical or thermal loads acting on the equipment due to typical working conditions in the subsea installations (such as pressure, temperature, bending, currents, waves, vortex induced vibrations, accidental loads etc.) and residual stresses from welding as described in Section 2.2. .

High hydrogen concentration: Subsea systems with cathodic protection applied are exposed to hydrogen molecules, which tend to enter voids and cracks in the protected surface and increase its concentration over time. The electrons traveling through the water to the cathode cause the separation of positive hydrogen ions from water. Hydrogen ions can then enter the microstructure of the protected object [10].

Susceptible microstructure: Duplex steel is a HISC susceptible material. Its susceptibility to HISC has been shown to be strongly correlated to austenite spacing. A finer austenite spacing provides more resistance to HISC [11].

The hydrogen embrittlement process is illustrated in Figure 5. The process starts with hydrogen blistering where hydrogen molecules tend to enter micro-level voids of the CP protected equipment. Over time, the concentration of hydrogen increases, causing the rise in pressure, which after reaching a certain threshold can initiate cracking (see Figure 7). In the end, hydrogen embrittlement will occur when the hydrogen molecules having penetrated the micro cracks of the surface layer, can react with the surrounding material, forming compounds with far lower mechanical strength. Typically, the material becomes more brittle, which in return can cause chipping and erosion [12].

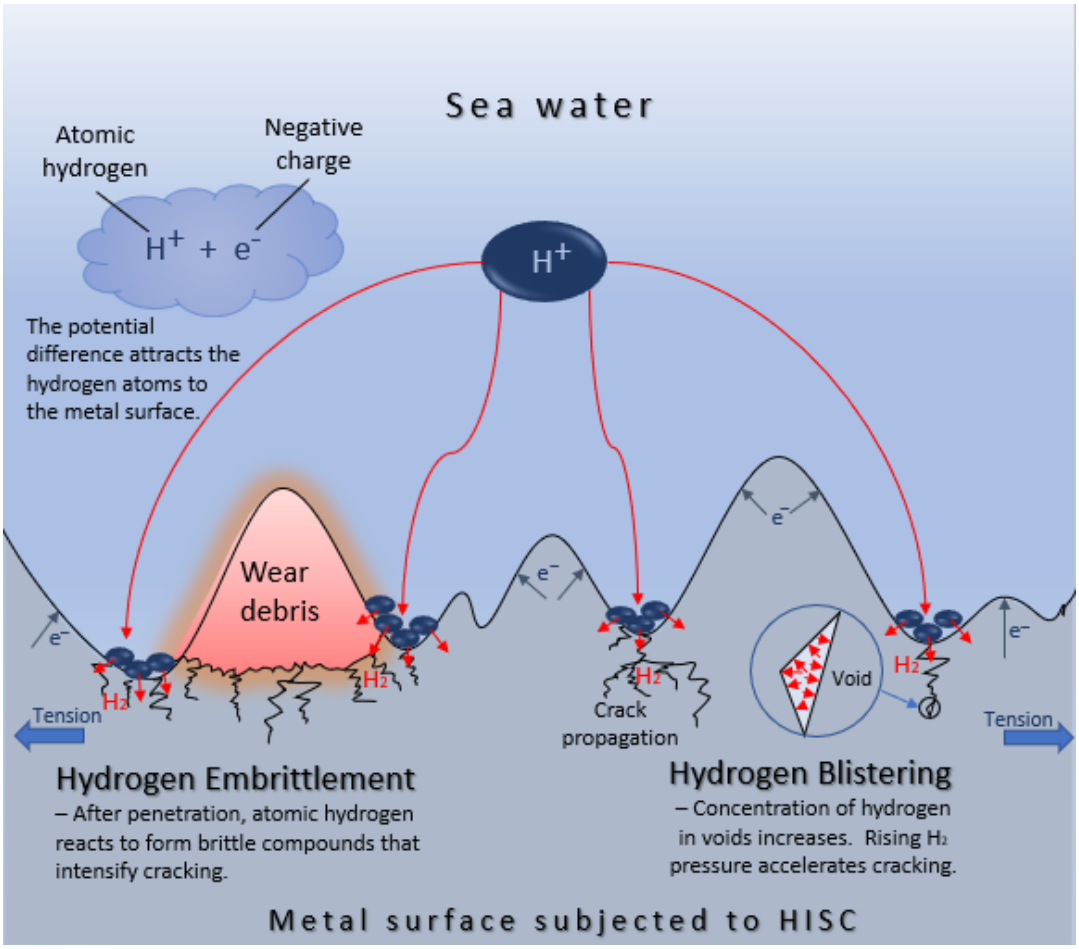

Figure 5. Schematic view of hydrogen embrittlement process

An example of an electron microscope scan of intergranular cracking due to hydrogen embrittlement in Duplex steel is presented in Figure 6.

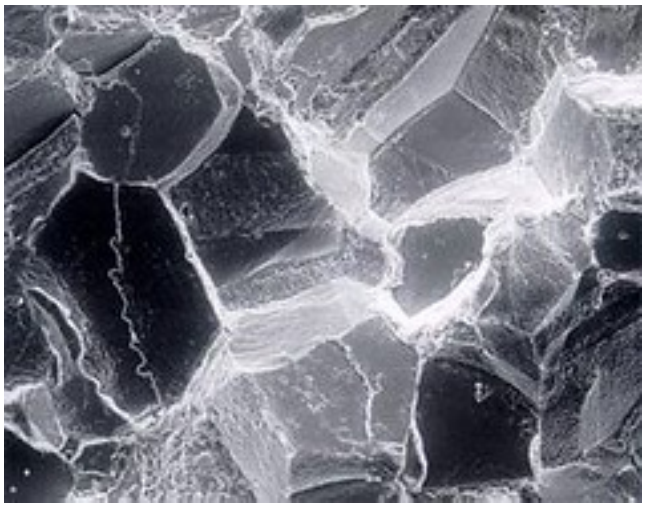

Figure 6. Hydrogen embrittlement example – electron microscope scan of an intergranular cracking (Weining Zhong, 2018, Creative Commons)

Another example of a crack propagation due to HISC in Duplex steel is presented in Figure 7.

Figure 7. Example of crack propagation due to HISC embrittlement (Uwe Arang, 2014, Creative Commons)

3. Mathematical theory

3.1. Simplified mathematical model of a welding process

In this paper, the welding process will be described as a moving source of heat with a specified dimensions and power as illustrated in Figure 8. The coordinate system in Figure 8 follows that of Goldak & Akhlaghi [13]. The power source is double ellipsoidal and is modelled using an external power density function. The power density function is listed in equation (1) and illustrated in Figure 9.

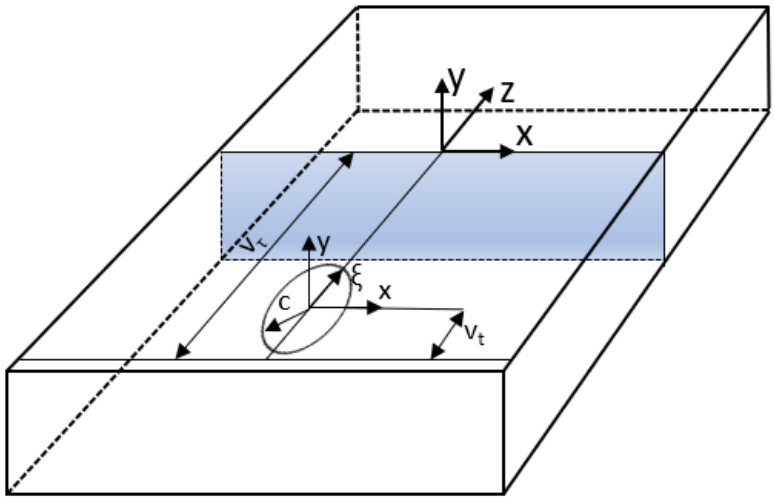

Figure 8. Implemented system of coordinates, used for the welding simulation

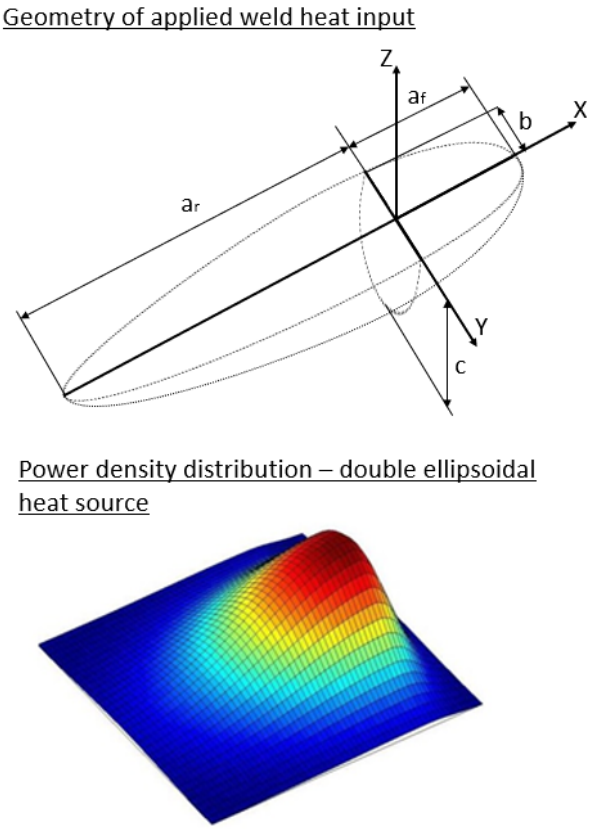

Figure 9. Geometry of the chosen mathematical model, Power density distribution using double ellipsoidal heat source model from Abid et al. [14]

$$q(x,y,z,t) = \frac{6\sqrt{3}Q}{abc\pi\sqrt{\pi}}\, e^{-3x^2/a^2}\, e^{-3y^2/b^2} e^{-3[z+vt]^2/c^2} \quad (1)$$

Where Q is the heat power flux [W], a is the length of the heat source [m], b is the width of the heat source [m], c is the height of the heat source [m], x is the width coordinate [m], y is the length coordinate [m], z is the height coordinate [m], v is the welding speed [m/s] and t is the time variable [s] [15].

The model is solved using a transient-thermal FE analysis in Ansys 2020 R1 [16].

3.2. Temperature gradient in the weld temperature profile

As mentioned previously, steeper temperature gradients lead to higher residual stress levels. The definition of the temperature gradient is presented in Figure 10.

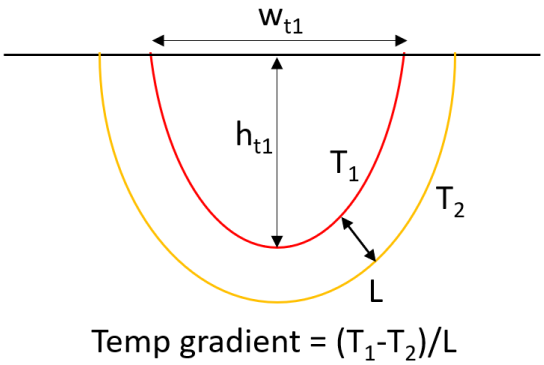

Figure 10. Width, height, and temperature gradient of the weld temperature profile

3.3. Pearson parametric correlation

In this paper, the Pearson correlation method is used. The Pearson Correlation Coefficient $\rho_{X,Y}$ values can be interpreted as follows:

- $\rho_{X,Y}$ close to 1 – strong positive linear correlation
- $\rho_{X,Y}$ close to 0 – no correlation
- $\rho_{X,Y}$ close to -1 – strong negative linear correlation

The Pearson correlation coefficient is given by:

$$\rho_{X,Y} = \frac{cov(X,Y)}{\sigma_X \sigma_Y} \quad (2)$$

where $cov(X,Y)$ is the covariance of X and Y range, σ_X is the standard deviation of X and σ_Y is the standard deviation of Y. To understand the influence of the atmospheric conditions on the HAZ, the simulations and correlation matrix will be solved for both moderate climate conditions and winter arctic conditions. A sample size of 200 is used in this paper.

An example of a parametric correlation study is Xing et al. [17] where a subsea carbon fibre composite pipeline subjected to internal pressure loadings was studied.

4. FE Simulation

4.1. Model geometry

The model chosen for analysis is a 200 mm long solid bar with rectangular cross section with width and height of 40 mm and 10 mm, respectively and is presented in Figure 11.

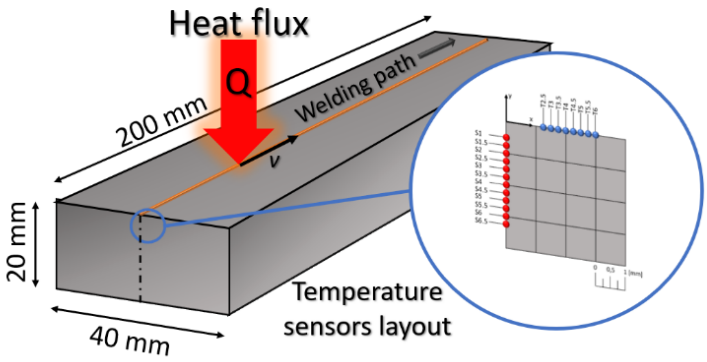

Figure 11. Illustration of the model geometry with the welding path (See Figure 12 for temperature sensor arrangement)

4.2. Temperature measurement points

Sensors were located at the surface and center of the model section, which should allow for monitoring of heat penetration (12 sensors) and surface spread (8 sensors). This sensor arrangement is illustrated in Figure 12.

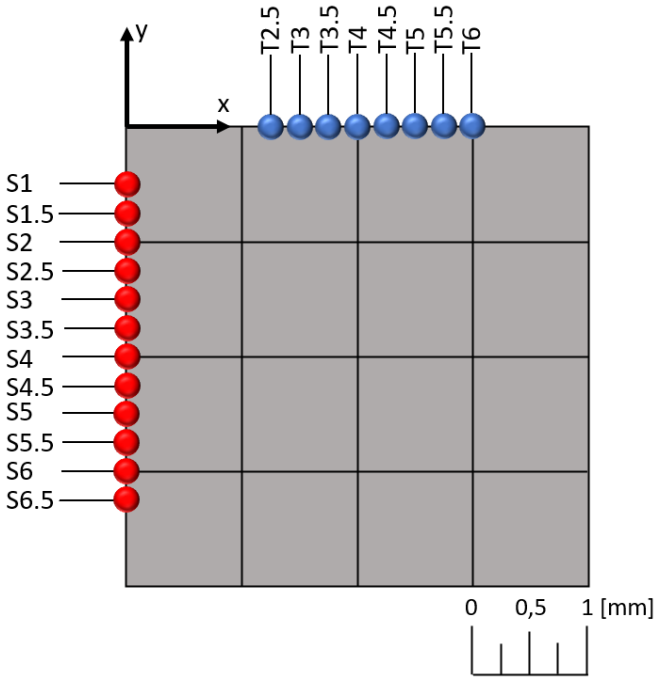

Figure 12. Temperature sensor arrangement

4.3. Loads and boundary conditions

The thermal load (weld heat flux) applied to the model depends on heat flux power (Q), heat source dimensions (a, b and c), as well as welding speed (v). As illustrated in the Figure 11, the heat flux will move in a translatory motion, following a path on the surface of the metal flat bar.

The boundary conditions are illustrated in Figure 13 and include convection and heat flow. Convection is assigned to 5 faces of the model geometry – 1 top and 4 side surfaces. The bottom surface

is defined with the heat flow condition. It is perfectly insulated, therefore heat flow cannot penetrate the bottom of the model.

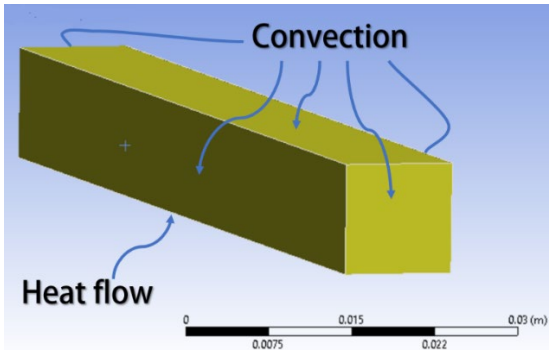

Figure 13. Assignment of boundary conditions to the model faces

4.4. Parameters studied

The parameters studied and their corresponding ranges are presented in Table 2.

Table 2. Parameters studied and corresponding ranges

Parameter	Symbol	Unit	Min value	Max value
Heat flux power	Q	W	1150	1402
Length of heat source	a	m	3.60×10^{-3}	4.40×10^{-3}
Width of heat source	b	m	3.60×10^{-3}	4.40×10^{-3}
Height of heat source	c	m	3.60×10^{-3}	4.40×10^{-3}
Welding speed	v	m/s	4.50×10^{-3}	5.50×10^{-3}
Convection film coefficient	h	$Wm^{-1}K^{-1}$	90	110
Convective ambient temperature	T_{AC}	°C	19.8	24.2
Density	ρ	kgm^{-3}	7072	8634
Thermal conductivity	κ	$Wm^{-1}K^{-1}$	54	67
Specific heat	C_p	$Jkg^{-1}K^{-1}$	391	477

4.5. Mesh refinement study

A mesh refinement study is performed to verify if the finite element mesh is sufficiently fine. The results are presented in Table 3. A total of six simulation cases were performed for a variety of mesh configurations. For example, a mesh configuration of 50 x 5 x 5 means that the length, width, and height of the plate are divided into 50, 5 and 5 intervals, respectively. This means that there are 50 elements along the length, 5 elements along the width and 5 elements along the height. This corresponds to a element size of 4 x 4 x 4 mm which is listed as the cell size in Table 3. The maximum temperature obtained in the transient heat analysis is used as the compared variable in the study. The results showed that a 200 x 20 x 20 mesh configuration with a 1 x 1 x 1 mm cell size gives a 0.2 % error. This mesh is used for the rest of the paper.

Table 3. Results of mesh refinement study

Sim no.	Mesh config	Cell size [mm]	Maximum temp [°C]	Error
1	50 x 5 x 5	4 x 4 x 4	1045.8	17.7%
2	100 x 10 x 10	2 x 2 x 2	1176.4	7.4%
3	150 x 15 x 15	1.3 x 1.3 x 1.3	1259.6	0.8%
4	**200 x 20 x 20**	**1 x 1 x 1**	**1272.4**	**0.2%**
5	250 x 25 x 25	0.8 x 0.8 x 0.8	1270.1	0.0%
6	300 x 30 x 30	0.5 x 0.5 x 0.5	1270.2	Reference

An example of heat distribution plot for selected mesh configuration (200 x 20 x 20) is presented in Figure 14.

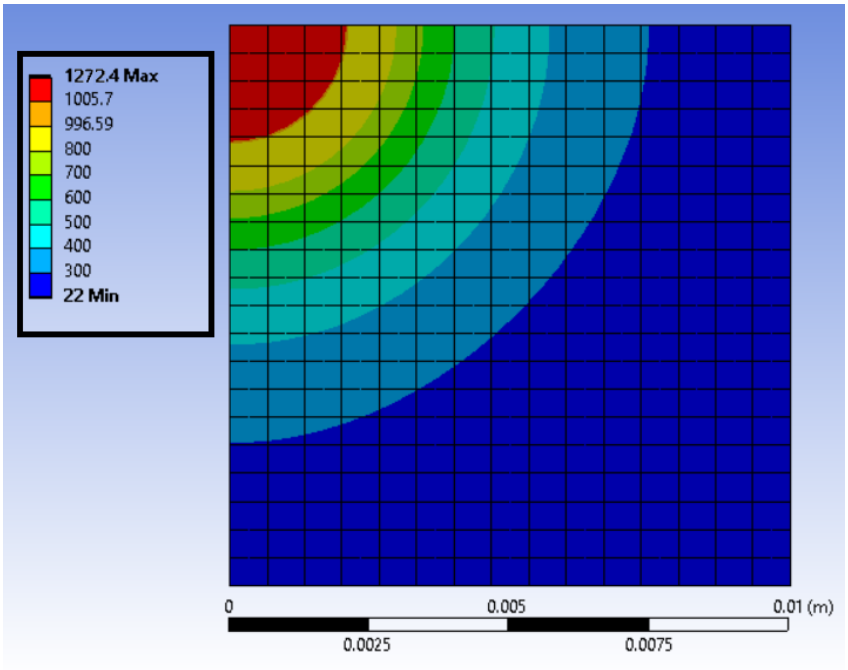

Figure 14. Temperature distribution in the model cross section - heat flux load

5. Results and discussions

5.1. Parameter correlation analysis

The parameter correlation matrices are presented in Figure 15 and Figure 16 for the temperate and artic conditions, respectively. *Q, a, b, c, v, h, TAC, ρ, κ* and C_p were presented in Table 2. w800, d800, w1000, d1000, w1200 and d1200 are the width and height of the 800 °C, 1000 °C and 1200 °C temperature profiles, respectively and these are illustrated in Figure 10.

	Q	a	b	c	v	h	TAC	ρ	κ	cp	w800	d800	w1000	d1000	w1200	d1200
Q	1.00	0.01	-0.01	0.02	0.00	0.01	0.01	0.00	0.01	0.00	0.30	0.58	0.66	0.64	0.43	0.62
a	0.01	1.00	-0.02	0.01	0.00	0.01	0.01	0.04	0.00	0.02	-0.05	0.11	-0.21	-0.05	-0.19	-0.20
b	-0.01	-0.02	1.00	0.00	0.00	0.00	0.00	0.02	0.01	0.01	0.00	-0.22	-0.06	-0.27	-0.03	-0.30
c	0.02	0.01	0.00	1.00	0.00	0.00	0.00	-0.02	0.01	0.01	-0.09	-0.12	-0.20	-0.18	-0.10	-0.22
v	0.00	0.00	0.00	0.00	1.00	0.02	0.01	0.00	0.01	0.01	-0.04	-0.28	-0.28	-0.27	-0.20	-0.26
h	0.01	0.01	0.00	0.00	0.02	1.00	0.00	0.01	0.01	0.01	0.02	-0.01	-0.01	0.00	-0.02	0.00
TAC	0.01	0.01	0.00	0.00	0.01	0.00	1.00	0.00	0.01	0.00	0.05	-0.07	0.02	0.01	-0.06	0.02
ρ	0.00	0.04	0.02	-0.02	0.00	0.01	0.00	1.00	-0.01	-0.01	-0.03	-0.33	-0.28	-0.27	-0.27	-0.25
κ	0.01	0.00	0.01	0.01	0.01	0.01	0.01	-0.01	1.00	0.00	0.04	-0.26	-0.37	-0.37	-0.33	-0.38
cp	0.00	0.02	0.01	0.01	0.01	0.01	0.00	-0.01	0.00	1.00	-0.05	-0.31	-0.28	-0.25	-0.19	-0.25
w800	0.30	-0.05	0.00	-0.09	-0.04	0.02	0.05	-0.03	0.04	-0.05	1.00	0.18	0.24	0.31	-0.34	0.18
d800	0.58	0.11	-0.22	-0.12	-0.28	-0.01	-0.07	-0.33	-0.26	-0.31	0.18	1.00	0.77	0.75	0.58	0.75
w1000	0.66	-0.21	-0.06	-0.20	-0.28	-0.01	0.02	-0.28	-0.37	-0.28	0.24	0.77	1.00	0.86	0.66	0.85
d1000	0.64	-0.05	-0.27	-0.18	-0.27	0.00	0.01	-0.27	-0.37	-0.25	0.31	0.75	0.86	1.00	0.57	0.86
w1200	0.43	-0.19	-0.03	-0.10	-0.20	-0.02	-0.06	-0.27	-0.33	-0.19	-0.34	0.58	0.66	0.57	1.00	0.67
d1200	0.62	-0.20	-0.30	-0.22	-0.26	0.00	0.02	-0.25	-0.38	-0.25	0.18	0.75	0.85	0.86	0.67	1.00

Figure 15. Correlation of temperature curves dimensions with welding parameters – Temperate climate

	Q	a	b	c	v	h	TAC	ρ	κ	cp	w800	d800	w1000	d1000	w1200	d1200
Q	1.00	-0.01	0.01	0.00	0.00	0.01	0.01	0.01	-0.02	0.00	0.63	0.60	0.68	0.64	-0.04	0.61
a	-0.01	1.00	0.00	0.01	-0.01	0.00	0.02	-0.01	0.01	-0.01	-0.18	0.06	-0.21	-0.12	0.01	-0.15
b	0.01	0.00	1.00	-0.02	0.00	0.00	-0.02	0.00	-0.01	0.00	0.02	-0.12	-0.02	-0.21	0.04	-0.19
c	0.00	0.01	-0.02	1.00	-0.01	0.00	0.00	-0.01	-0.01	-0.01	-0.15	-0.09	-0.19	-0.18	-0.12	-0.17
v	0.00	-0.01	0.00	-0.01	1.00	0.01	0.00	0.01	0.00	0.00	-0.22	-0.30	-0.27	-0.29	0.01	-0.17
h	0.01	0.00	0.00	0.00	0.01	1.00	0.01	0.02	0.01	0.01	0.02	-0.06	0.02	-0.02	-0.03	-0.03
TAC	0.01	0.02	-0.02	0.00	0.00	0.01	1.00	-0.02	-0.01	-0.01	0.05	-0.01	0.06	0.03	0.00	0.00
ρ	0.01	-0.01	0.00	-0.01	0.01	0.02	-0.02	1.00	0.00	-0.01	-0.24	-0.30	-0.28	-0.27	0.08	-0.21
κ	-0.02	0.01	-0.01	-0.01	0.00	0.01	-0.01	0.00	1.00	0.00	-0.24	-0.35	-0.34	-0.40	-0.09	-0.39
cp	0.00	-0.01	0.00	-0.01	0.00	0.01	-0.01	-0.01	0.00	1.00	-0.30	-0.32	-0.27	-0.23	-0.08	-0.20
w800	0.63	-0.18	0.02	-0.15	-0.22	0.02	0.05	-0.24	-0.24	-0.30	1.00	0.69	0.77	0.78	-0.22	0.61
d800	0.60	0.06	-0.12	-0.09	-0.30	-0.06	-0.01	-0.30	-0.35	-0.32	0.69	1.00	0.79	0.77	0.01	0.70
w1000	0.68	-0.21	-0.02	-0.19	-0.27	0.02	0.06	-0.28	-0.34	-0.27	0.77	0.79	1.00	0.84	0.02	0.80
d1000	0.64	-0.12	-0.21	-0.18	-0.29	-0.02	0.03	-0.27	-0.40	-0.23	0.78	0.77	0.84	1.00	-0.03	0.76
w1200	-0.04	0.01	0.04	-0.12	0.01	-0.03	0.00	0.08	-0.09	-0.08	-0.22	0.01	0.02	-0.03	1.00	0.22
d1200	0.61	-0.15	-0.19	-0.17	-0.17	-0.03	0.00	-0.21	-0.39	-0.20	0.61	0.70	0.80	0.76	0.22	1.00

Figure 16. Correlation of temperature curves dimensions with welding parameters – Artic climate

In general, the correlation matrices for both temperate and artic climate conditions are similar. The following parameters were found to have stronger correlations to the final weld temperature profiles obtained.

- Heat flux power: Highest correlation with the temperature distributions. The correlation coefficients are mostly above 0.60 and therefore are relatively strong. Increasing the welding source power results in a deeper heat penetration and surface dissipation. Parameters describing the geometry dimensions of the heat flux have a negative correlation. Reduction of flux

dimensions results in volumetric power concentration; the outcome is a less uniform heat spread which could lead to increased susceptibility to HISC.

- Heat flux geometry and welding speed: Inversely correlated to the temperature distributions. The correlation coefficients are mostly above -0.30 and therefore are not particularly strong. Lowering welding speed allows the object to receive more thermal energy.
- Density, thermal conductivity, and specific heat: Inversely correlated to the temperature distributions. The correlation coefficients are mostly above -0.40 and therefore are not particularly strong. It is noted the uncertainties related to these material properties are usually very low. Therefore, for practical purposes, the variations caused by these parameters on the final welding results are typically low.

5.2. Temperature profile

The temperature profiles for both temperature and artic climate conditions for the mean parameter values presented in Table 2 are presented in Figure 17. The ambient temperature has a significant influence on the heat distribution during welding. For arctic conditions, the temperature curves are more densely concentrated and are located closer to the welded surface. The heat penetration is substantially reduced for the temperate climate conditions. At room temperature the heat has a much wider radial spread both on the surface and depth of the welded material. Steeper temperature gradient along the z axis and model surface results in an increased concentration of residual stresses after cooling down. ambient temperature is important and should also be taken into consideration in the welding optimization.

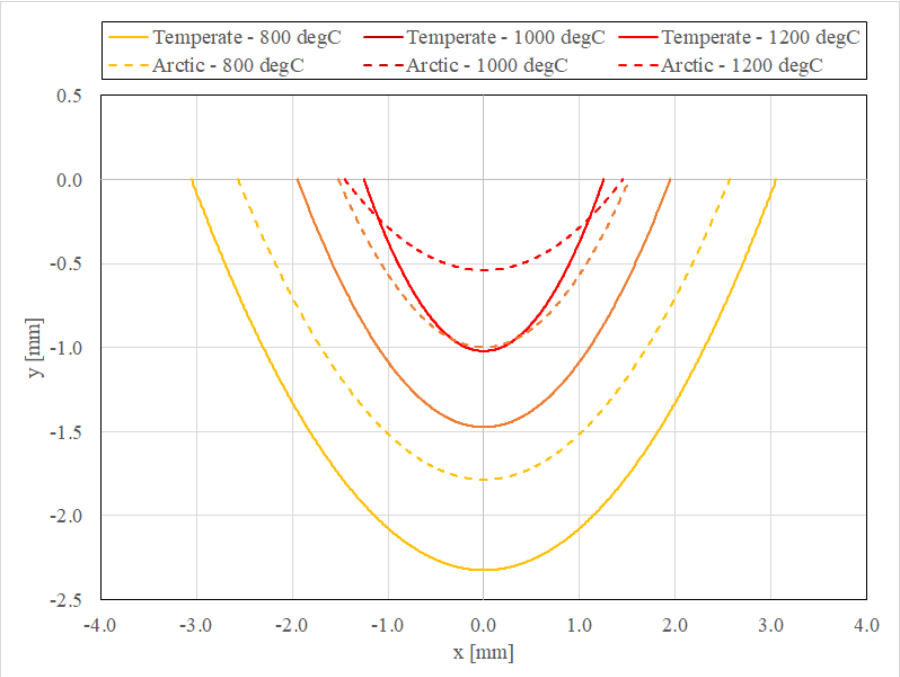

Figure 17. Comparison of temperature distribution for temperate (dotted line) and arctic (continuous line) climate conditions.

6. Conclusions

The aim of this paper is to understand the influence of welding parameters on the welding process of Duplex steels in artic climates in relation to susceptibility to HISC. Susceptibility to HISC is indicated by the temperature gradients measured from the temperature profiles as discussed in Section 3.2. . A steeper temperature gradient indicates a higher susceptibility to HISC. FE transient-heat analyses of the welding process were performed for a wide variety of welding parameters. Parametric correlation

analyses were carried out on the results to obtain the correlation between the parameters. Furthermore, the temperature profile comparisons were also performed. The study was carried out for both temperate (22°C) and artic (-45°C) climate conditions.

The results show that heat flux power has the largest influence on the weld temperature profile. Other parameters that have a relatively large influence are the heat flux geometry, welding speed, density, thermal conductivity, and specific heat of the metal. It is also shown that welding in the cold artic conditions leads to steeper temperature gradients due to a more rapid cool down which can in turn increase the susceptibility to HISC.

References

[1] Salvio F, Silva B and Silva dos Santos D 2013 On the role of HISC on Super and hyper duplex stainless steel tubes, *Proc. Offshore Tech. Conf* (Rio de Janerio: May 6 – 9, 2013).
[2] Bahrami A and Woollin P 2010 Hydrogen induced stress cracking of duplex stainless steel subsea components, *Proc. 29th Int. Conf. Offshore Mech. Arct. Eng.* (Shanghai: Jun 6 - 11, 2010).
[3] Stannard D M and Warburton A 1993 Duplex stainless steel: Specification requirements, *Proc. 25th Offshore Tech. Conf* (Houston, May 3 - 6, 1993).
[4] Byrne G, Francis R and Warburton G 2016 Hydrogen induced stress Cracking (HISC) resistance and improvement methods for super duplex stainless steels, *Proc. Corrs. 2016* (Vancover, Mar 6 – 10, 2016).
[5] Aucott L 2015 *Mechanism of Solidification Cracking during Welding of High Strength Steels for Subsea Linepipe* (United Kingdom: Leicester University).
[6] Ren X, As S, Nyhus B and Akselsen O 2012 Residual stresses of X80 pipe girth weld, *Proc. 22nd Int. Soc. Offshore Polar Eng.,* (Rhodes, Jun 17 – 22, 2012).
[7] Adedayo A, Ibitoye S and Oyetoyan A 2010 Annealing heat treatment effects on steel welds, *J. Miner. Mater. Charact. Eng.* **9**(6), 547-57
[8] Todinov M 2007 Generic solutions for reducing the likelihood of overstress and wearout failures", Book chapter in *Risk-Based Reliability Analysis and Generic Principles for Risk Reduction.*
[9] TubingChina.com 2019 *Avoid PWHT Post Weld Heat Treatment*, Assessed 10.11.2019 from https://tubingchina.com/Avoid-PWHT-Post-Weld-Heat-Treatment.htm
[10] DNV-RP-F112 2010 *Duplex Stainless Steel – Design against Hydrogen Induced Stress Cracking, Recommended Practice.*
[11] Zhang W 2016 Evaluation of susceptibility to hydrogen embrittlement - A rising step load testing method, *Mater. Sci. Appl.* **7**(8), 389-395.
[12] Woollin P and Gregori A 2004 Avoiding hydrogen embrittlement stress cracking of ferritic austenitic stainless steels under cathodic protection, *Proc. 23rd Conf. Offshore Mech. Arct. Eng.* (Vancouver, Jun 20 - 25, 2004).
[13] Di Benedetti M, Loreto G, Matta F and Nanni A 2013 Acoustic emission monitoring of reinforced concrete under accelerated corrosion, *J. Mater. Civ. Eng.* **25**(8), 1022-29.
[14] Abid M, Wajid H A and Ullah S 2015 Parametric study for residual stresses and deformations in welded pipe flange joints, *Iran. J. Sci. Technol. Trans. Mech. Eng.* **39**(2), 427-36.
[15] Goldak J and Akhlaghi M 2005 *Computational Welding Mechanics.* (New York: Springer).
[16] Ansys R2020 2020 *Theory Manual.*
[17] Xing Y, Xu W and Buratti V 2019 The correlation and determination matrices associated with the burst design of a subsea carbon-fibre-epoxy composite flow-line, *Proc. of 2nd COTech Conf.* (Stavanger: Nov 27 – 29, 2017) Eds H G Lemu et al. (IOP Conference Series: Material Science and Engineering) vol 700.